SEPTEMBER 01 2023

In-process volumetric sensing of defects in multiple parts during powder bed fusion using ultrasound

Nathan J. Kizer; Corey J. Dickman; Abdalla R. Nassar ; Edward W. Reutzel ; Christopher M. Kube

JASA Express Lett. 3, 094001 (2023)
https://doi.org/10.1121/10.0020739

JASA EXPRESS LETTERS ARTICLE asa.scitation.org/journal/jel

In-process volumetric sensing of defects in multiple parts during powder bed fusion using ultrasound

Nathan J. Kizer,[1] Corey J. Dickman,[2] Abdalla R. Nassar,[2] Edward W. Reutzel,[1,2] and Christopher M. Kube[1,a)]

[1]Department of Engineering Science and Mechanics, The Pennsylvania State University, University Park, Pennsylvania 16802, USA

[2]Applied Research Laboratory, The Pennsylvania State University, State College, Pennsylvania 16804, USA

njk19@psu.edu, cjd160@arl.psu.edu, NassarAbdallaR@JohnDeere.com, ewr101@arl.psu.edu, kube@psu.edu

Abstract: This letter reports on the integration of eight ultrasonic transducers into a build substrate for individual in-process monitoring of eight parts fabricated using powder bed fusion additive manufacturing. Ultrasound is shown to be able to sense poor fusion of parts to the substrate and also sensitivity to porosity. This technique demonstrates the utility of ultrasound as one of a few techniques able to interrogate the volume of additively manufactured parts during the process. Additionally, the ability to measure several parts during a single build can be used for efficient process parameter development studies, as the ultrasonic measurements can offer rapid information about part quality and integrity.

[Editor: Régis Marchiano] https://doi.org/10.1121/10.0020739

Received: 1 June 2023 **Accepted:** 31 July 2023 **Published Online:** 1 September 2023

1. Introduction

As metal additive manufacturing (AM) advances, there arises a need to monitor parts during the printing process. The final part performance is highly dependent on the process parameters used during fabrication and can result in many undesired defects, such as porosity, which inhibits part performance.[1,2] Optimal values of process parameters, such as laser power and laser speed in fusion-based AM, are determined for each new metal powder feedstock through trial and error using sacrificial builds. Advancements in metal AM are slowed by the traditional route of building and subsequent characterization to determine ideal process parameters. Ultimately, these factors result in significant material waste and energy usage, in addition to time and labor costs. One example of a high-cost material is 9Cr1Mo stainless steel (Gr91), which has been proposed as a candidate for laser additive processes for the application of nuclear reactors due to its high-temperature creep resistance.[3] To the best of our knowledge, Lienert and Maloy reported the first instance of metal powder bed fusion using Gr91 powder.[4]

In situ powder bed fusion (PBF) monitoring has been of interest in recent years. Many techniques have focused on monitoring melt pool characteristics. Techniques based on optical cameras, thermography, and pyrometers can view the exposed portion of the melt pool during the process. Lack of fusion beneath the surface has been inferred from detected melt pool anomalies, but the likelihood of false and/or missed indications is significant.[5,6] Two major limitations of such monitoring methods are that the imaging is throttled by the frame rate of the camera equipment and is severely limited due to the inability to detect defects beneath the topmost surface.

Acoustic techniques are emerging as sensing modalities in AM settings. Previous work on ultrasonic inspection of AM parts indicates the potential of using ultrasound during the process to gain insight on defect formation and melt pool behavior. Ultrasound was used to detect pore networks within AM parts and estimate grain size for wrought stainless steels.[7,8] Nonlinear ultrasound has also been conducted on additively manufactured parts to characterize the microstructure.[9] When considering *in situ* implementation, previous attempts have been made to integrate ultrasonic and acoustic monitoring. Rieder *et al.* mounted a transducer under the build substrate of a powder bed fusion printer to monitor a single sample with intentional regions of porosity.[10] Sotelo *et al.* monitored samples produced through hybrid directed energy deposition for pores.[11] Bakre *et al.* utilized noncontact laser ultrasound to generate Rayleigh waves to monitor Ti64 samples during a directed energy deposition process.[12] Kube *et al.* utilized ultrasonic shear waves to monitor the evolution of laser-generated melt pools.[13] Gillespie *et al.* built upon this by monitoring melt pools using oblique ultrasonic waves and mapping melt pool features to simultaneously acquired X-ray images.[14] Shevchik *et al.* utilized acoustic emission sensors to differentiate between porosity concentrations within printed samples.[15] Ultrasound inspection for defect detection and

a)Author to whom correspondence should be addressed.

characterization has been widely accomplished. These examples support the potential of using ultrasound for process parameter development. However, simultaneous monitoring of multiple individual samples using ultrasound has not been accomplished previously to the best of our knowledge. This letter reports on the development, integration, and testing of a multi-channel ultrasonic system for monitoring multiple individual Gr91 parts simultaneously during powder bed fusion. Samples were manufactured with different laser power and speed combinations, which allowed us to assess the ultrasonic sensitivity to the resulting part structure. The ability to assess multiple individual parts at once enables the possibility of using ultrasound to automatically optimize processing parameters. The nondestructive character of ultrasound could substantially reduce material waste and eliminate costly destructive characterization. In addition, *in situ* ultrasonic sensing is considered a viable tool to assess sonochemistry methods that aim to positively influence the melt pool and resulting properties of AM parts using acoustic excitation.[16,17]

2. Methodology

This section first details the modifications made to the printer to enable monitoring, fabrication parameters for the parts, and ultrasonic sensing details. Ultrasound was integrated into the powder bed fusion process by installing ultrasonic transducers into the build chamber. Before modification of the printer, the build chamber housed a 50.8 mm–thick build substrate made from 1045 steel bolted onto a heated build plate to control the temperature of the build substrate during printing. For the experiments detailed herein, the heated build plate was installed into the assembly but was not activated to prevent interference with the integrated *in situ* monitoring equipment. A modified build substrate was fabricated to contain thermocouples and ultrasonic sensors. A $155.6 \times 155.6\,\text{mm}^2$ cavity was milled from the center with an overhanging lip toward the bottom of the substrate. A 9.53 mm recess was also milled to place a stainless steel insert over the sensors. The insert was made from wrought Gr91 stainless steel to match the Gr91 powdered feedstock and had dimensions $152.4 \times 152.4 \times 9.53\,\text{mm}^3$. A 3D printed fixture made from polylactic acid (PLA) filament was printed and placed within the modified build substrate cavity, as shown in Fig. 1(a). The fixture was designed to contain nine ultrasonic sensors, but only eight were used during the experiments. The transducer housings were placed centered with the print locations of the samples to avoid unwanted reflections from sample edges. Each transducer housing contained a spring that pressed the transducer to the insert after fastening it to the modified substrate. The springs intended to form uniform coupling to the plate with about 22–44 N of pressure on each transducer. A high-temperature couplant was used between the transducer/insert interface, which is resistant to evaporation since temperatures within the cavity can reach up to 70 °C. In each cavity corner, 12.7 mm cylindrical cutouts were machined to house ceramic washers and bushings where the PLA fixture rested to isolate it from the metal substrate. Four thermocouples were placed in the fixture along with the ultrasonic transducers. The thermocouples collected temperature information at the bottom surface of the insert and the ambient temperature within the cavity. A 64-channel Explorer ultrasonic phased array (The Phased Array Company, West Chester, OH) was used to control eight piezoelectric transducers (ndtXducer, Northborough, MA) with center frequency and element diameter of 10 MHz and 12.7 mm, respectively. The sampling and pulse rate frequencies of the transducer were 100 MHz and 28.57 kHz, respectively. The phased array operated each transducer in pulse-echo mode, for which the same transducer sends and receives an ultrasonic pulse. In general, the transducers were set up to excite sequentially and independently from each other so that the signals do not interfere. A particular transducer began pulsing when a start trigger event was sent from the printer, which provided control of when each transducer would be active. The depiction of the transducer monitoring a test build and the nine test samples is shown in Fig. 1.

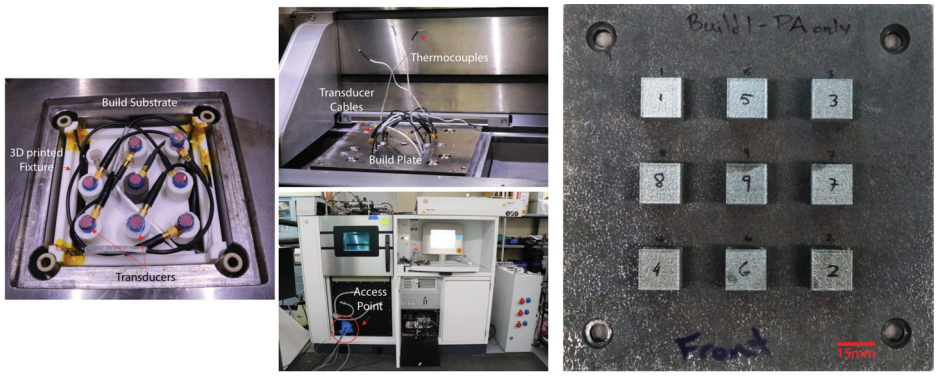

Fig. 1. (a) Ultrasonic sensors within the substrate cavity with 3D printed fixture (left). Wiring path through the EOS M280 printer for the ultrasonic cables and transducers (right). (b) Actual build insert and printed samples.

Table 1. Chemical composition of the Gr91 metal feedstock powder. Composition was collected using inert gas fusion (ASTM E 1019-18), combustion infrared detection (ASTM E 1019-18), and direct current plasma spectroscopy (ASTM E 1097-12).

Element	O	N	C	S	Si	Mn	P	Cr	Ni	Mo	V
Weight %	0.027	0.051	0.097	0.004	0.34	0.45	0.017	8.91	0.16	0.95	0.19
Element	Cu	W	Al	B	Ti	Nb	As	Sb	Sn	Pb	Zr
Weight %	0.049	0.005	0.014	<0.0005	0.0204	0.082	<0.001	<0.002	0.005	<0.001	<0.002

The AM process utilized an M280 powder bed fusion printer (EOS, Germany) using Gr91 metal powder feedstock (Hoeganaes Specialty Metal Powder, Cinnaminson, NJ) with a particle diameter ranging between 20–63 μm. The chemistry of the powder (Luvak Laboratories, Boylston, MA) is shown in Table 1.

Nine samples with a cross sectional area of $15.88 \times 15.88\,\text{mm}^2$ and 12.7 mm in height were printed on the build insert with a spacing of 18 mm arranged in a square grid. A range of laser power and speed combinations between 200–250 W and 500–800 mm/s, respectively, was chosen in an effort to induce different structures amongst the parts. Table 2 shows the respective processing parameters for the samples.

All other processing parameters, including the distance between laser passes, or hatch spacing ($h = 120$ μm) and layer height ($d = 40$ μm), were held constant during the build. The laser parameters were guided by those used by Lienert and Maloy for Gr91 builds using powder bed fusion.[4] Often, the volumetric energy density (VED) is employed as a normalized processing parameter metric,

$$\Psi = \frac{P}{vhd}. \tag{1}$$

For the present build, the VED values are given in Table 2. The VED for a set of process parameters is an important metric to consider since it is related to the energy input from the melt laser. The VED of the laser parameters has been correlated to defects within additively manufactured Ti-6Al-4V samples.[18] Despite this, the energy density, on its own, may not be a good indicator of material quality across a wide range of process parameters. Thus, it is important to report VED in addition to the explicit laser power and speed parameters.[19] While the results reported in this letter will be correlated to VED, the primary connections of the results to porosity are the relative densities obtained from the Archimedes method and optical imaging.

Ultrasonic measurements were performed at three different instances for each sample within each build layer. First, measurements were performed for each sample as the laser was present on the respective sample. This resulted in collecting data for 1.5 s or 42 857 waveforms per sample per layer. These time series measurements were focused on melt pool monitoring and will be the focus of future work.[14] The second set of measurements was performed after the lasing process was complete for each sample but before the recoater deposited new powder to print the subsequent layer. In this case, the top surface of each sample was exposed to the build chamber environment. Two virtual samples were placed into the printing protocol to give additional time for the samples to cool prior to recoating. In this case, waveforms were collected for 0.1 s, with all eight transducers exciting and receiving waveforms sequentially, resulting in 2857 waveforms collected from each sample. After a set pause time at the end of the recoating process, a third set of measurements was performed after the printer deposited and spread a new layer of powder on the print bed. These measurements were done to assess the uniformity of powder spreading over the sample. After the samples were printed and removed from the build substrate, optical microscopy and x-ray computed tomography (μCT) were conducted on the cut surfaces and through the thickness of the samples.

3. Results and discussion

The current letter focuses on the second set of measurements, collected when the laser was not active and prior to powder spreading, as described in the previous section. These measurements are the simplest case since the samples have a top surface free of powder and the temperature variation was minimized from one layer to the next. In general, ultrasonic waves are capable of propagating through several inches in metallic samples at MHz frequencies if the samples are homogeneous. If defects like pores or delaminations are present in the sample, a portion of the ultrasonic wave will scatter or

Table 2. The speed (v), power (P), and volumetric energy density (Ψ) used to build each sample.

Sample #	1	2	3	4	5	6	7	8	9
Speed (mm/s)	600	600	600	600	500	800	800	800	700
Power (W)	250	250	200	225	250	200	225	250	250
Ψ (J/mm^3)	86.8	86.8	69.4	78.1	104.2	52.1	58.6	65.1	74.4

reflect at the boundary of these heterogeneities. In turn, the reflections can be measured using the same sensor as the generating wave. These general attributes of ultrasound were leveraged in the present work to detect formation of heterogeneities during the printing process. The build surface on top of the insert seen in Fig. 1(b) was fabricated using the same Gr91 alloy as the metal feedstock powder. The longitudinal and shear wave speeds of wrought Gr91 stainless steel were calculated at room temperature using a standard cross correlation process and were determined to be 5840 m/s and 3256 m/s, respectively.[20] From these wave speed values, the bulk and shear moduli of wrought Gr91 can be calculated to be 155.8 and 82.7 GPa, respectively. The insert is a standard wrought plate and homogeneous. Thus, perfect fusion of the part and the insert will eliminate any distinct interface between the part and insert that could obfuscate the ultrasound measurements. In this situation, the transmission of ultrasound into the part will be optimal. In practice, an observed ultrasonic reflection will indicate poor fusion or a delamination at the joint between the part and insert. If not all of the energy is reflected, a transmitted wave will be able to propagate up into the part and probe heterogeneities within the part. Ultrasonic waves are sensitive to heterogeneities that are larger or on the same order of magnitude as the wavelength of the propagating wave. The 2857 waveforms collected at each layer for each respective sample were then averaged into a single waveform, which removes Gaussian random noise. Thus, this process results in a single waveform for each layer and 317 overall waveforms for each sample because each sample consisted of 317 layers. To visualize how the averaged waveforms evolved as a function of build height of the samples, the average time amplitude waveform at each layer are arranged as seen in Fig. 2. These plots are known as b-scans, or brightness-scans, as the colors indicate the amplitude of the waveforms. Samples 1–9 are shown in the subplots of Fig. 2, in which the absolute values of the averaged waveforms are

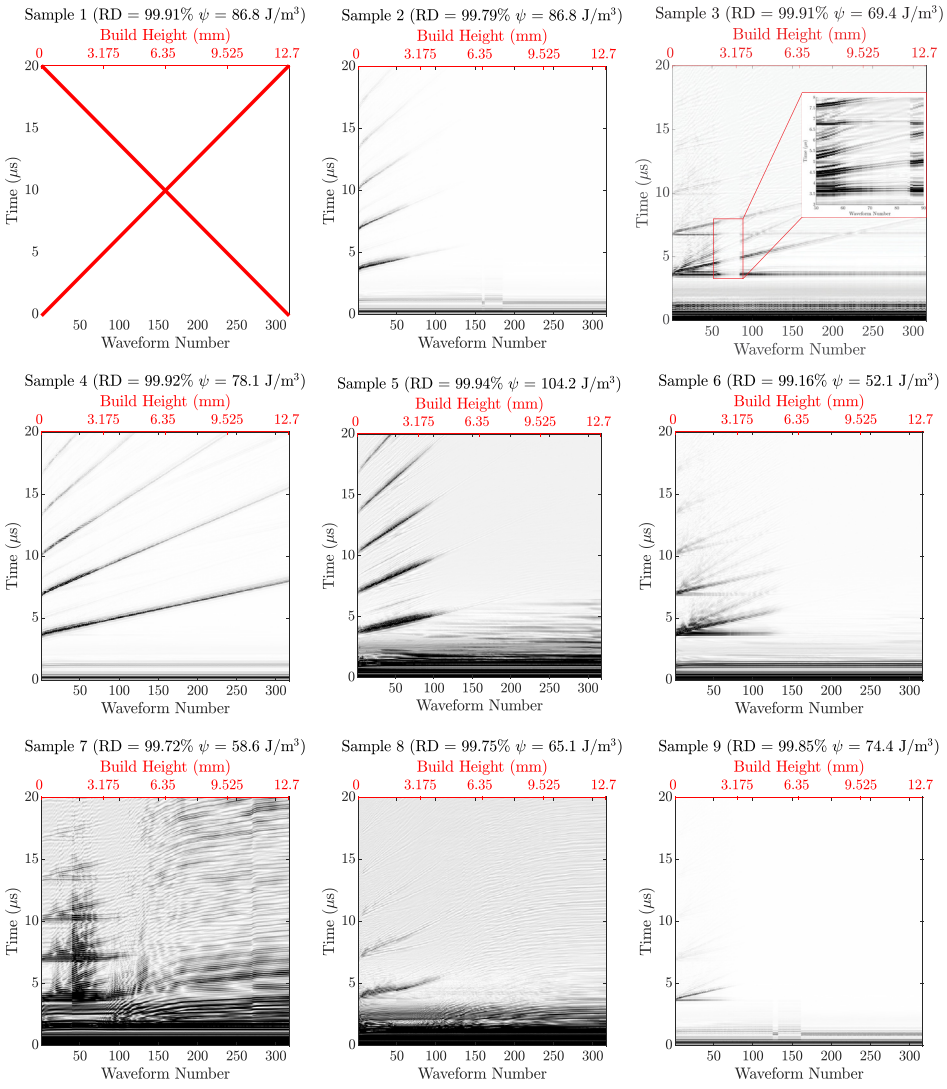

Fig. 2. Amplitude plots for samples 1–9 collected during printing. The darker regions on the plots indicate a higher amplitude of the transducers receiving the reflected wave.

included to enhance vertical resolution. Based on the amplitudes and arrival times of the ultrasonic reflections, we can seek evidence of echoes stemming from heterogeneities such as poor joining at the insert/part interface or porosity in the sample. The initial reflection at 3.3 μs from the first averaged waveform is the reflection between the insert/part interface. This reflection time agreed with the expected value using the longitudinal wave speed of 3.26 μs and known insert thickness of 9.53 mm. The 0.07 μs difference is expected from microscale uncertainty of the couplant and transducer wear plate thickness and wave-speed measurement. By focusing on this arrival time, samples 2, 4, and 5 all share common features indicating good fusion, such as high amplitude reflections within the first 100 layers. The reflections are linearly increasing in arrival time meaning that waves are propagating largely unperturbed through the thickness of the samples and reflecting from the respective top surfaces. This trend in reflection was expected since the layer height for each layer was consistent. Multiple repeated reflections can also be seen within these samples. Samples 3, 6, 8, and 9, however, give different reflection trends. Close to the first expected arrival time for the initial reflections, a split in reflection amplitude can be seen for these samples. One portion of the response is similar to samples 2, 4, and 5 with good transmission while the other portion remains constant in arrival time as build height increases. The initial split from the first reflection is a sign that the ultrasonic waves are scattering from heterogeneities within the initial layers of the print. Fewer internal reflections are also present within these samples when compared to samples 2, 4, and 5. It should also be noted that the vanishing signals present in samples 2, 5, 6, 8, and 9 are suspected to be attenuation differences caused by defects within the sample and/or uneven pressure between transducers and insert, which caused an uneven application of couplant. The evidence of uneven couplant application is apparent in Fig. 1(a). For example, for sample 9 (the transducer in the center of the fixture), there is little couplant remaining on the face of the transducer, indicating that the couplant had been pushed out. The transducers for samples 4 and 6 both have even layers of couplant left over after the insert was removed; so, the variability in couplant is not of concern for these samples.

Sample 1 was not connected to an ultrasonic sensor; therefore, no data were collected during the experiments. Sample 7 shows indications of high signal saturation, due to user error in setting initial gain values. In the b-scan for sample 3, there is a decrease in the amplitude between layers 60 and 85. This phenomenon is still unknown, and further work is being done to interpret the result. Using the trends observed in the ultrasonic scans, valuable insights can be made about determining the optimal values of volumetric energy density. Table 3 shows Ψ for all samples and their relative densities (RD) measured by the Archimedes method. It should be noted that there is about a 0.08% error in relative density with the Archimedes method.[21] Samples 2, 4, and 5, which had indications of good fusion, all had Ψ of greater than 75 J/mm^3. Samples 3, 6, 8, and 9 were signaled to have poor fusion based on ultrasound and have Ψ less than 75 J/mm^3. As shown in Table 3, the samples with Ψ greater than 75 J/mm^3 sometimes have lower relative densities than samples fabricated with Ψ less than 75 J/mm^3. That is to say, unlike the ultrasonic measurements, the density measurements show no clear trend in the presence of heterogeneities within the samples with respect to the Ψ values. Further results will support that ultrasound could identify "good" vs "poor" samples.

Of the eight samples printed and monitored by ultrasound, samples 4 and 6 were compared in more detail, as shown in Fig. 3. For sample 4, the ultrasonic signal's arrival was plotted vs the waveform number, which linearly increased with build height. The analysis is focused on the first 70 layers of each sample due to the artifacts appearing early in the build. A gradual shift in the arrival was observed as the samples were printed. This trend was expected for a sample that shows no apparent defects, such as regions of high porosity or a delamination that could scatter the ultrasonic signal. Ultrasonic waves have been shown to be sensitive to porous regions within a sample as observed by Rieder *et al.*[10] In other words, the waves are propagating undisturbed through the build insert and the thickness of sample 4 with no apparent signs of defects. However, faint reflections are observed in sample 4 between arrival times 3.6 and 3.8 μs that appear throughout the scan time. The amplitude of the reflections is smaller than what is expected out of a defect which could be a sign of sensitivity to smaller microstructural features. For sample 6, early reflections that did not shift in time were detected in the build's initial layers indicating that the ultrasonic waves are scattering from heterogeneities within the sample. Reflections are observed from the top surface, similar to sample 4, but these have a smaller amplitude. The appearance of the top surface reflections indicates that the waves still propagate through the heterogeneities within the sample without scattering considerable energy. The earliest indication of disturbance shown in Fig. 3(b) was around 3.4 μs, which aligns with a heterogeneous region being present within the initial layers of the sample.

After printing, samples 4 and 6 were sectioned from the insert and polished for optical microscopy. Figures 3(c) and 3(d) show the optical images from each sample's cut surface. A wire electrical discharge machine (EDM) was used to remove as little material as possible during part removal. The cut for samples 4 and 6 occurred where the constant reflections were observed from the earliest response in the sample 6 ultrasonic data at about layer 7. The optical imaging

Table 3. Density of each sample relative to fully dense Gr91 stainless steel bar stock.

Sample #	1	2	3	4	5	6	7	8	9
Relative density (%)	99.91	99.79	99.91	99.92	99.94	99.16	99.72	99.75	99.85
Ψ (J/mm^3)	86.8	86.8	69.4	78.1	104.2	52.1	58.6	65.1	74.4

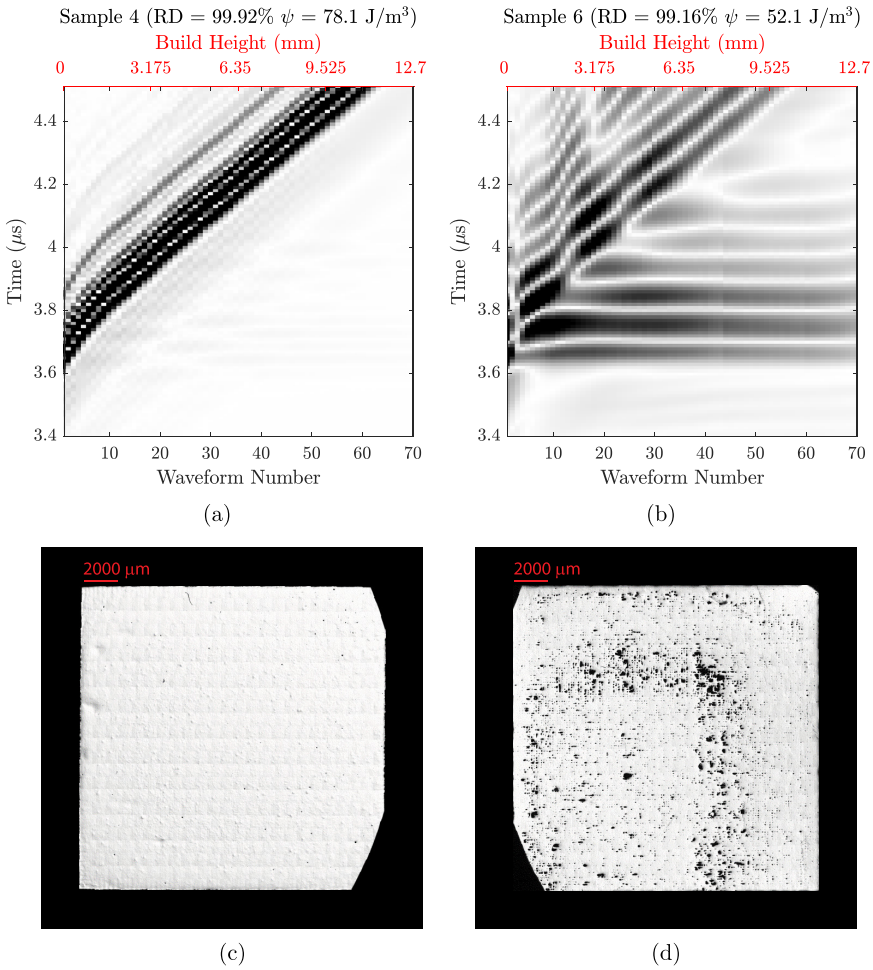

Fig. 3. Optical microscopy images of (a) sample 4 and (b) sample 6, in addition to their respective ultrasound images in (c) and (d).

corroborates what was observed with the ultrasonic data showing that sample 4 has little indication of porosity. Sample 6 shows an indication of porosity throughout the cut plane. The networked pores on the interface caused the observed ultrasonic response. Although the ultrasonic equipment is not sensitive to single pores that are less than 100 μm in diameter, networked pores are an agglomeration of connected pores and are more readily detected.[22] Further sectioning of sample 6, in Fig. 4, was also done along the build direction showing porosity throughout the sample, which revealed porosity present

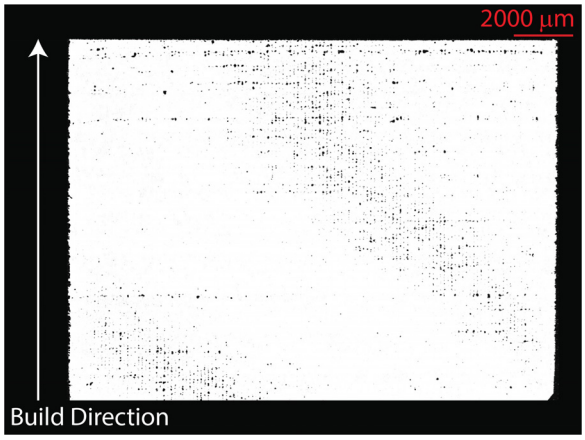

Fig. 4. Optical image of the cut interface through the thickness of sample 6.

throughout the sample's thickness. Despite sample 6 having a relative density of 99.16%, pore networks have been shown to be present through the thickness of the sample. The ultrasonic signal was sensitive to the pores near the build surface and throughout the thickness. The consistent porosity throughout the thickness of sample 6 indicates that the pores were due to the laser parameters as opposed to the powder feedstock. The pores present within the sample had sharp edges and irregular shapes, which is a characteristic of lack of fusion porosity.[22] Sample 6 was documented to have the lowest VED of the samples printed, which correlated to the sample's lack of fusion porosity.

4. Conclusions

A modified build substrate for a powder bed fusion metal 3D printer was used to house ultrasonic sensors to monitor samples during printing. Eight samples with varying laser speed and power were monitored during the process. The samples were then destructively tested using optical microscopy to determine whether porosity was present. Multiple samples could be inspected during the printing process using a modified operation of an ultrasonic phased array system. The ultrasonic equipment was able to differentiate samples with different volumetric energy densities through *in situ* monitoring, whereas relative density measurements did not show a definite relationship with volumetric energy density. The experiments indicated that samples with lower volumetric energy densities showed indications of lack of fusion porosity which was detectable by the ultrasonic equipment and corroborated by the optical microscopy images. Progress toward determining optimal process parameters for powdered Gr91 stainless steel was made based on the characterization of samples produced in this experiment. Future work includes determining the layer thickness consistency throughout the print bed to estimate accuracy relative to the prescribed layer thickness along with real-time melt pool monitoring during the lasing process.[14]

ACKNOWLEDGMENT

This research is being performed using funding received from the DOE Office of Nuclear Energy's University Programs under Grant No. DE-NE0008995.

AUTHOR DECLARATIONS

Conflict of Interest

There are no conflicts of interest related to this work.

DATA AVAILABILITY

The data that support the findings of this study are available from the corresponding author upon reasonable request.

References

[1]M. Grasso and B. M. Colosimo, "Process defects and *in situ* monitoring methods in metal powder bed fusion: A review," Meas. Sci. Technol. **28**, 044005 (2017).
[2]A. Leicht, M. Rashidi, U. Klement, and E. Hryha, "Effect of process parameters on the microstructure, tensile strength and productivity of 316L parts produced by laser powder bed fusion," Mater. Charact. **159**, 110016 (2020).
[3]V. K. Sikka, Development of Modified 9 Cr-1 Mo Steel for Elevated-Temperature Service, Report no. CONF-830659-16 (Oak Ridge National Laboratory, 1983).
[4]T. J. Lienert and S. A. Maloy, "Laser Additive Manufacturing of F/M Steels for Radiation Tolerant Nuclear Components," Report no. LA-UR-17-30052 (Los Alamos National Laboratory, 2017).
[5]J. Bamberg, G. Zenzinger, and A. Ladewig, "In-process control of selective laser melting by quantitative optical tomography," in *19th World Conference on Non-Destructive Testing*, Germany (2007).
[6]F. Bayle and M. Doubenskaia, "Selective laser melting process monitoring with high speed infra-red camera and pyrometer," in *Proceedings Volume 6985, Fundamentals of Laser Assisted Micro- and Nanotechnologies*, St. Petersburg, Russia (2008).
[7]O. Cook, N. Huang, R. L. Smithson, C. M. Kube, A. Beese, and A. P. Argüelles, "Ultrasonic characterization of porosity in components made by binder jet additive manufacturing," Mater. Eval **80**, 37–44 (2022).
[8]P. Palanichamy, A. Joseph, T. Jayakumar, and B. Raj, "Ultrasonic velocity measurements for estimation of grain size in austenitic stainless steel," NDT&E Int. **28**, 179–185 (1995).
[9]A. Bellotti, J.-Y. Kim, J. E. Bishop, B. H. Jared, K. Johnson, D. Susan, P. J. Noell, and L. J. Jacobs, "Nonlinear ultrasonic technique for the characterization of microstructure in additive materials," J. Acoust. Soc. Am. **149**, 158–166 (2021).
[10]H. Rieder, M. Spies, J. Bamberg, and B. Henkel, "On- and offline ultrasonic characterization of components built by SLM additive manufacturing," AIP Conf. Proc. **1706**, 130002 (2016).
[11]L. D. Sotelo, R. Karunakaran, C. S. Pratt, M. P. Sealy, and J. A. Turner, "Ultrasound *in situ* characterization of hybrid additively manufactured Ti6Al4V," J. Acoust. Soc. Am. **150**, 4452–4463 (2021).
[12]C. Bakre, T. Meyer, C. Jamieson, A. R. Nassar, E. W. Reutzel, and C. J. Lissenden, "In-situ laser ultrasound-based Rayleigh wave process monitoring of DED-AM metals," Res. Nondestruct. Eval. **33**, 218–242 (2022).
[13]C. M. Kube, Y. Shu, A. J. Lew, and D. Galles, "Real-time characterization of laser-generated melt pools using ultrasound," Mater. Eval. **76**, 525–534 (2018).

[14]J. Gillespie, W.-Y. Yeoh, C. Zhao, N. D. Parab, T. Sun, A. D. Rollett, B. Lan, and C. M. Kube, "*In situ* characterization of laser-generated melt pools using synchronized ultrasound and high-speed X-ray imaging," J. Acoust. Soc. Am. **150**, 2409–2420 (2021).
[15]S. A. Shevchik, C. Kenel, C. Leinenbach, and K. Wasmer, "Acoustic emission for in situ quality monitoring in additive manufacturing using spectral convolutional neural networks," Addit. Manuf. **21**, 598–1921 (2018).
[16]H. Ohrdes, S. Nothdurft, C. Nowroth, J. Grajczak, J. Twiefel, J. Hermsdorf, S. Kaierle, and J. Wallaschek, "Influence of the ultrasonic vibration amplitude on the melt pool dynamics and the weld shape of laser beam welded EN AW-6082 utilizing a new excitation system for laser beam welding," Prod. Eng. **15**, 151–160 (2021).
[17]C. J. Todaro, M. A. Easton, D. Qiu, D. Zhang, M. J. Bermingham, E. W. Lui, M. Brandt, D. H. StJohn, and M. Qian, "Grain structure control during metal 3D printing by high-intensity ultrasound," Nat. Commun. **11**, 142 (2020).
[18]H. Gong, K. Rafi, H. Gu, T. Starr, and B. Stucker, "Analysis of defect generation in Ti-6Al-4V parts made using powder bed fusion additive manufacturing processes," Addit. Manuf. **1–4**, 87–98 (2014).
[19]K. G. Prashanth, S. Scudino, T. Maity, J. Das, and J. Eckert, "Is the energy density a reliable parameter for materials synthesis by selective laser melting?," Mater. Res. Lett. **5**, 386–390 (2017).
[20]J. F. Costa-Júnior, G. A. Cortela, L. E. Maggi, T. F. D. Rocha, W. C. A. Pereira, R. P. Costa-Felix, and A. V. Alvarenga, "Measuring uncertainty of ultrasonic longitudinal phase velocity estimation using different time-delay estimation methods based on cross-correlation: Computational simulation and experiments," Measurement **122**, 45–56 (2018).
[21]A. B. Spierings, M. Schneider, and R. Eggenberger, "Comparison of density measurement techniques for additive manufactured metallic parts," Rapid Prototyping J. **17**, 380–386 (2011).
[22]Z. Snow, A. R. Nassar, and E. W. Reutzel, "Invited review article: Review of the formation and impact of flaws in powder bed fusion additive manufacturing," Addit. Manuf. **36**, 101457 (2020).